OPEN ACCESS

GAVIN PUBLISHERS

Biosensors and Bioelectronics Open Access

Research Article

Xu L, et al. Biosens Bioelectron Open Acc: BBOA-136.

DOI: 10.29011/ 2577-2260. 100036.

An Electrochemical DNA Sensor for Ultrasensitive Detection of Aspirin Resistance Gene Based on Signal Amplification Strategy of $Ru(NH_3)_6^{3+}$/MPA/Cys Redox Cycling

Lili Xu[2], Naiqiang Zhuo[1], Xiaobo Lu[1*],Yongxian Wan[1]

[1]Department of Orthopedics, affiliated Hospital of Southwest Medical University, Luzhou, China

[2]Department of rehabilitation Medicine, affiliated Hospital of Southwest Medical University, Luzhou, China

[*]**Corresponding author:** Xiaobo Lu, Department of Orthopedics, PROOF affiliated Hospital of Southwest Medical University, No. 20 of Taiping Street in the Jiangyang district, Luzou city, Sichuan province, P. R. China. Tel: +86-8313165451; Fax: +86-8313165451 Email: wyx20170820@163.com

Citation: Xu L, Zhuo N, Lu X, Wan Y (2018) An Electrochemical DNA Sensor for Ultrasensitive Detection of Aspirin Resistance Gene Based on Signal Amplification Strategy of $Ru(NH_3)_6^{3+}$/MPA/Cys Redox Cycling. Biosens Bioelectron Open Acc: BBOA-136. DOI: 10.29011/ 2577-2260. 100036.

Received Date: 21 May, 2018; **Accepted Date:** 04 June, 2018; **Published Date:** 11 June, 2018

Abstract

Aspirin resistance, the phenomenon of patient showing no response to aspirin, is characterized by a predominant mutation in the COX-1 gene. Accordingly, patients are routinely screened for mutations in this gene to determine whether they can benefit from aspirin treatment. In this work, we reported a simple and ultrasensitive electrochemical method for COX-1 C50T detection for the first time based on Electrochemical-Chemical-Chemical (ECC) redox cycling. In the procedure of assay, $Ru(NH_3)_6^{3+}$ is used as the electron acceptor that is electrostatically attracted to Peptide Nucleic Acid (PNA) modified electrodes and new chemical regents of Mercaptopropionic Acid (MPA) and cysteamine were introduced, which permits $Ru(NH_3)_6^{3+}$ to be regenerated for multiple redox cycles. Different Pulse Voltammetry (DPV) was applied to record the electrochemical signals, which increased linearly with the target DNA. Under optimal conditions, the DNA sensors showed a wide linear relationship, from 10 fM to 1 nM, with detection limits of 2.8 fM (S/N = 3). This strategy paves a new avenue for the determination of aspirin resistance gene in patient serum.

Keywords: Aspirin Resistance; COX-1; DNA Sensor; Electrochemical-Chemical-Chemical

Introduction

After more than a century, aspirin is one of the most commonly used drugs in western medicine for the prevention of cardiovascular diseases [1]. Despite adequate aspirin therapy, 6.2% to 57% patients still experience cardiovascular events, the phenomenon named as Aspirin Resistance (AR) [2]. Researchers have reported that genetic variability in Cyclooxygenase-1 (COX-1) C50T affect aspirin response with cardiovascular disease and could be used as specific genetic marker of AR [3,4]. Therefore, it is crucial to prescreen patients for their genotypes before prescribing aspirin to facilitate target therapy and decreasing the side effects associated with prolonged administration.

Various methods have been developed for the detection of the COX-1 mutation at the DNA level. Among them is the Polymerase Chain Reaction (PCR) or DNA sequencing [5,6]. DNA sequencing is an excellent approach for research studies that seek to profile large regions of DNA, but its implementation is prohibitively expensive for routine clinical use and the slow turnaround time (2-3 weeks) is not an ideal for optimal treatment outcomes.[6] Also, PCR is prone to interference from the components of biological samples and requires purification of the nucleic acids from samples. Therefore, a method that is simpler, and able to detect rare mutations directly in serum, is required urgently.

In recent years, a versatile platform for markers detection has been developed based on DNA sensors, owing to their low cost and potential for high levels of multiplexing and sensitivity [7]. This type of testing approach has been applied successfully to the analysis of

a subset of antibiotic resistance [8], but the feasibility of analysing resistance gene for anticoagulant drug in clinical samples has not been established. Here we explored the feasibility of applying this technology to direct analysis of the aspirin resistance gene COX-1 from patient serum samples. To minimize the background current and increase the signal-to-noise ratio, a neutral charge biotinylated Peptide Nucleic Acid (PNA) probe complementary to the target sequence was selected to modify the electrode surface [9,10]. For accomplishing the low abundance sequence detection, streptavidin was further introduced during DNA sensor fabrication. Because it can provide more active sites for the immobilization PNA probe [11,12]. In order to immobilization more streptavidin, reduced Graphene Oxide–Tetraethylene Pentamine (rGO–TEPA) and Gold Porous Nanoparticles (Au PNPs) were integrated [13-15].

Electrochemical-Chemical-Chemical (ECC) redox cycling can be used to amplify signals produced at DNA modified electrode surfaces to increase the sensitivity and accuracy of a detection assay [16-18]. In the procedure of assay, $Ru(NH_3)_6^{3+}$ acts as a redox label and binds to DNA nonspecifically through electrostatic interactions with the phosphate backbone, and therefore, the electrochemical reduction of this species yields a signal that reports on the increase of negatively charged groups at the electrode surface upon hybridization of a target sequence [19]. In addition, to overcome the interfering redox reactions near the potential of interest and amplify signals, new chemical regents of MPA and Cys were introduced, which permits Ru(III) to be regenerated for multiple redox cycles [20]. In recent years, although promising research has produced DNA sensors using ECC redox cycle reporter system to detect mutated nucleotides in samples, to the best of our knowledge, this is the first reported use of DNA sensors for the detection COX-1 gene, a biomarker implicated aspirin resistance.

Expérimental

Chemicals and Materials

Reduced Graphene Oxide – Tetraethylene Pentamin (rGO-TEPA) was provided by Nanjing XFNANO Materials TECH Co., Ltd. (China). Tris-(2-Carboxyethyl)-Phosphine Hydrochloride (TCEP), Gold (Ⅲ) Chloride Trihydrate ($HAuCl_4 \cdot 3H_2O$), streptavidin, 6-Mercaptohexanol (MCH), $Ru(NH_3)_6Cl_3$, 3-Mercaptopropionoic Acid (MPA), Cysteamine (Cys), were obtained from Sigma-Aldrich (St. Louis, USA, www. Sigma-Aldrich. com). Potassium Ferricyanide ($K_3Fe(CN)_6$) and Potassium Ferrocyanide ($K_4Fe(CN)_6$) were purchased from Beijing Chemical Reagents Company (Beijing, China). Clinical serum samples were obtained from a local hospital and stored at 4°C. Biotinylated Peptide Nucleic Acid (PNA) probes were synthesized and purified by Shanghai RuiDi Biological Technology Co., Ltd. The sequences of PNA probes are as follows: 5'-Bio-Cys-O-ATC-ATC-CTG-ACT-GGC-ATC-CGG-3', where Bio represents biotin, O represents an ethylene glycol linker and Cys represents the amino acid cysteine. Other oligonucleotides were also synthesized and purified by Shanghai RuiDi Biological Technology Co., Ltd. with their sequences illustrated in Table S1.

Nucleotide name	Sequence (5'→3')
PNA	Bio-Cys-O-ATC-ATC-CTG-ACT-GGC-ATC-CGG
Target DNA	CCG-GAT-GCC-AGT-CAG-GAT-GAT
Single-base mismatch	CCG-GAT-GGC-AGT-CAG-GAT-GAT
Three-base mismatch	CCG-GAT-GGC-AGT-CTG-GTT-GAT
Non-complementary	GGC-TGA-GGC-TAC-GGC-ACT-G

Table S1: Synthetic oligonucleotide sequences in this study.

The buffer solutions involved in this study were as follow: 1 × TE buffer (10 mM Trishydroxymethylaminomethane hydrochloride (Tris-HCl), and 1.0 mM Ethylenediaminetetraacetic Acid (EDTA), pH 8.0), which was used to dissolve all oligonucleotides. Phosphate Buffered Solution (PBS) (pH 7.4, 0.1 M) was prepared with NaH_2PO_4 and Na_2HPO_4. Tris buffer solution (50 mM, pH 9) was obtained from Sigma-Aldrich (St. Louis, USA, www. Sigma-Aldrich. com). All other reagents were of analytical reagent grade and used without further purification. Ultrapure water (>18.2 ΩM) obtained from a Millipore Mill-Q purification system was used throughout the experiment.

Instruments

All electrochemical experiments were carried out on a CHI660E electrochemical workstation (Chenhua Instruments Co., Shanghai, China). Scanning Electron Microscopy (SEM) images were obtained by using a Hitachi S-3000N (Hitachi Limited, Japan). Field Emission Scanning Electron Microscopy (FE-SEM) image was conducted using a Hitachi S4800 (Hitachi Limited, Japan). Transmission Electron Microscopy (TEM) investigations were performed on a Hitachi Limited, Japan). A conventional three-electrode system was used for all electrochemical measurements: a Ag/AgCl reference electrode and a Pt counter electrode, and the modified Glassy Carbon Electrode (GCE, 4-mm in diameter) as the working electrode. A one-compartment cell fitted with a Luggin capillary was used to separate the working compartment from the reference compartment. Quantitative real-time Polymerase Chain Reaction (qRT-PCR) experiments were performed on a Light Cycler Nano Real Time PCR Instrument (Roche, UK).

Preparation of Porous Au Nanoparticles

Porous Au NPs were synthesized referencing to the literature [21,22]. Briefly, 1 M KOH solution (0.05 mL), 10 mM

fresh ascorbic acid (3 mL) aqueous solution, and 2 mL H_2O were sequentially injected into a conical flask. Then 2 mM Gold (III) chloride trihydrate solution (4 mL) was added. The mixture was blended for about 1min and then located in 60^0c thermostated container for 1 h. The resulting Au PNPs were centrifuged and washed with absolute ethanol and deionized-distilled water for thrice and then dispersed in 2 mL Milli-Q water.

Construction of DNA Sensors

The fabrication procedure of the electrochemical DNA biosensor is illustrated in Scheme 1. Prior to use, GCE was polished repeatedly using 0.3- and 0.05-µm alumina slurries followed by thorough rinsing with Milli-Q water. After successive sonication in baths of Milli-Q water, absolute alcohol and Milli-Q water again, the electrode was dried at room temperature. After that, 10 µL of rGO-TEPA (2 mg mL^{-1}) was cast onto the electrode surface and dried in the air. Subsequently, the electrode was immersed in porous Au nanoparticles solution and connected to CHI660E workstation using a three-electrode set-up with a Ag/AgCl reference electrode and a Pt counter electrode.

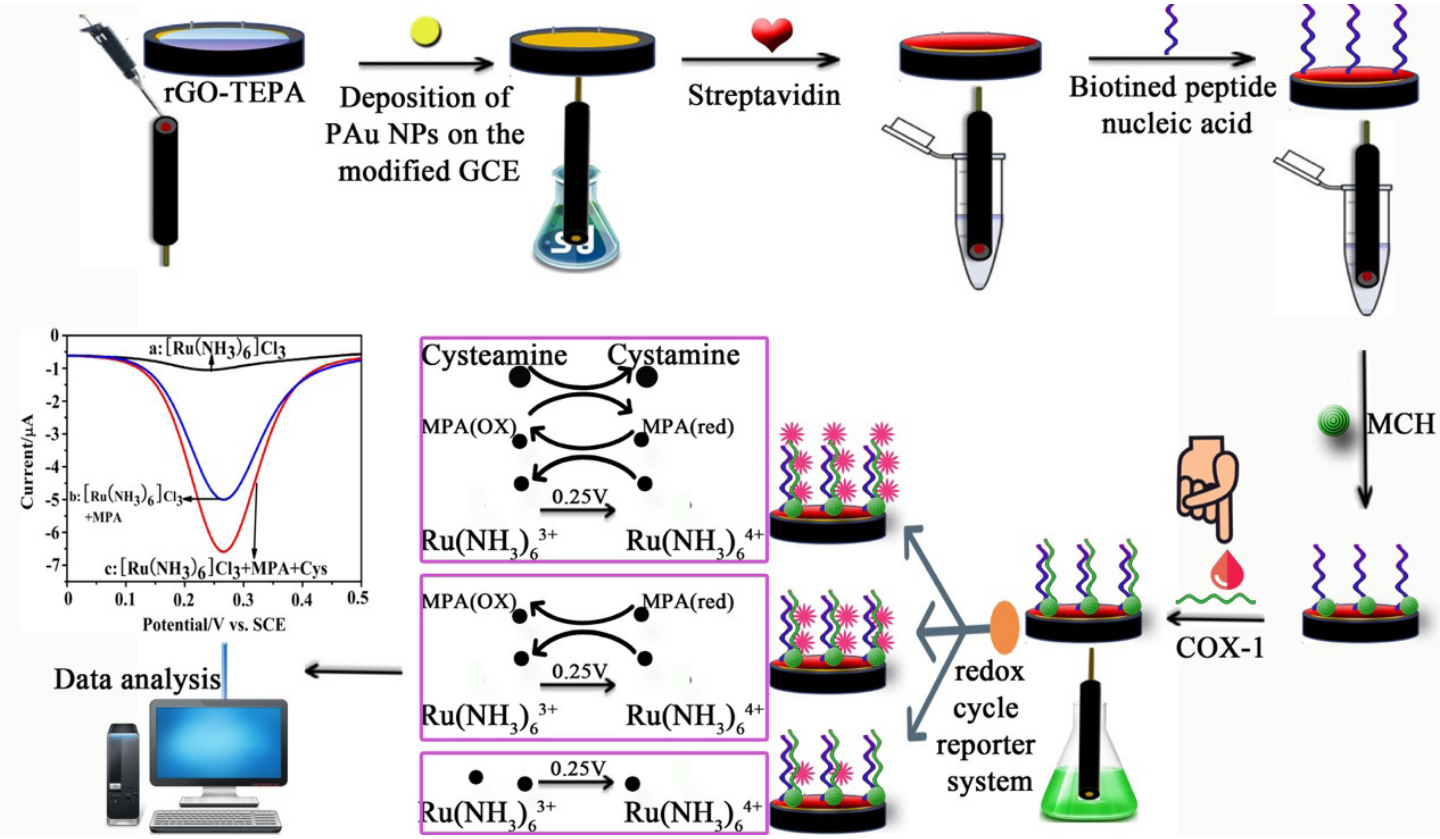

Scheme 1: Schematic illustration of the electrochemical DNA bioassay protocol.

Au PNPs were electrochemically deposited onto the rGO-TEPA-modified GCE surface under a constant potential of -0.2 V for 30 s. After washing with Milli-Q water, 10 µL of a streptavidin solution (100 ng mL^{-1}) was dropped onto the modified electrode surface through the strong effect of Au-NH_2 bonding to immobilize streptavidin. The electrode was kept at 4°C for 16 h, as streptavidin can retain its bioactivity for a long period of time at this temperature. After the reaction, the electrodes were washed with Milli-Q water to remove loosely bound chemicals and dried in nitrogen. After that, the device was covered with a EP lid.

Functionalization of DNA Sensors

An aqueous solution containing 1 µM of probe was mixed with 10 µM of aqueous Tris(2-carboxyethyl) phosphine hydrochloride solution and the mixture was left for overnight to cleave disulphide bonds. After that, 10 µL of probe solution was pipetted onto the sensors and incubated for 10 h in a dark humidity chamber at room temperature. Through the specific recognition between streptavidin and biotin, the biotinylated peptide nucleic acid probe was immobilized on the electrode surface for hybridization with target DNA. The sensors were then washed

thrice for 3 min with 0.1 × PBS at room temperature. The sensors were then treated with 1 mM of 6-Mercaptohexanol (MCH) for an hour at room temperature for back filling. After washing, the sensors were challenged with different concentration of targets for 60 min at room temperature. After hybridization, the sensors were washed thrice for 3 min with 0.1 × PBS at room temperature and the electrochemical scans were acquired.

Electrochemical detection of COX-1 DNA

All electrochemical experiments were carried out using CHI660E electrochemical workstation with a three-electrode system featuring a Ag/AgCl reference electrode and a platinum wire auxiliary electrode. The accumulation of $Ru(NH_3)_6^{3+}$ was measured by immersing PNA/DNA-modified electrodes in 10 μM $Ru(NH_3)_6Cl_3$ for 60 s, an amount of time where the cation would have equilibrated. By transferring to a Tris buffer solution (50 mM, pH 9) containing 10 μM $Ru(NH_3)_6Cl_3$, 0.5 mM 3-Mercaptopropionoic Acid (MPA) and 0.5 mM Cysteamine (Cys), Differential Pulse Voltammetry (DPV) signals were obtained with the potential range was from 0 V to 0.5 V, pulse amplitude of 50 mV, pulse width of 50 ms, and a pulse period of 100 ms. Signal changes that correspond to specific targets were calculated with background-subtracted currents: change in current (ΔI) = I_{after} - I_{before}, where I_{after} = current after target binding and I_{before} = current before target binding.

Results and discussion

Principle of this Method

We use a multi-pronged strategy to minimize the current in the absence of target nucleic acid. The sensors are functionalized with biotinylated Peptide Nucleic Acid (PNA) probes complementary to the target sequence. PNA is a synthetic nucleic acid analogue that has a neutral charge. This neutral charge minimizes the background current and increases the signal-to-noise ratio. Our new assay employs $Ru(NH_3)_6^{3+}$, Mercaptopropionic Acid (MPA) and cysteamine. The $Ru(NH_3)_6^{3+}$ electron acceptor complex is positively charged and binds to the sensors at levels that corresponding to the amount of negatively charged nucleic acid. On the application of a potential at 250 mV, $Ru(NH_3)_6^{3+}$ is oxidized to $Ru(NH_3)_6^{4+}$, producing a measurable current that reports on the presence of the target DNA. However, the limited concentration of $Ru(NH_3)_6^{3+}$ localized at the bound target nucleic acids yields a small current. To provide maximal sensitivity for the detection of DNA hybridization, we introduced MPA, the MPA is neutral charge, and so it does not bind to the sensor, but presents in solution to chemically reduce $Ru(NH_3)_6^{4+}$ back to $Ru(NH_3)_6^{3+}$, allowing for multiple turnovers of $Ru(NH_3)_6^{3+}$, which generates a high electrocatalytic current. This signal is further amplified by cysteamine, another reduction agent, which is chemically oxidized to cystamine by reducing the oxidized form of MPA (R-S-S-R) back to its reduced form (R-SH).

Characteristics of the Modified Electrodes

The stepwise DNA sensors fabrication processes were investigated by SEM and FE-SEM. (Figure 1A, 1a) display the typical SEM and FE-SEM images of rGO-TEPA. It was confirmed that rGO-TEPA has a wrinkled paper-like structure. SEM of the rGO-TEPA/Au PNPs is shown in (Figure 1B). As seen, spherical nanoparticles were coated on the rGO-TEPA surface. (Figure 1b) displays a typical TEM image of Au PNPs, which clearly reveals Au PNPs has porous spherical morphology and the average size of the nanoparticles was approximately 30 nm. Upon immobilization of streptavidin, proteins are trapped on the surface of the rGO-TEPA/Au PNPs, and a blurry surface image was observed, distinct from that shown in (Figure 1B). This result is indicative of successful streptavidin bonding on the surface of the rGO-TEPA/Au PNPs. Afterwards, with the immobilization of the biotinylated PNA probe onto the rGO-TEPA/Au PNPs/streptavidin film, the modified nanostructure exhibited a crystal shape, as shown in (Figure 1D). This crystal shape is distinct from that shown in (Figure 1C), indicating that the biotinylated PNA probe was successfully introduced via specific recognition between streptavidin and biotin.

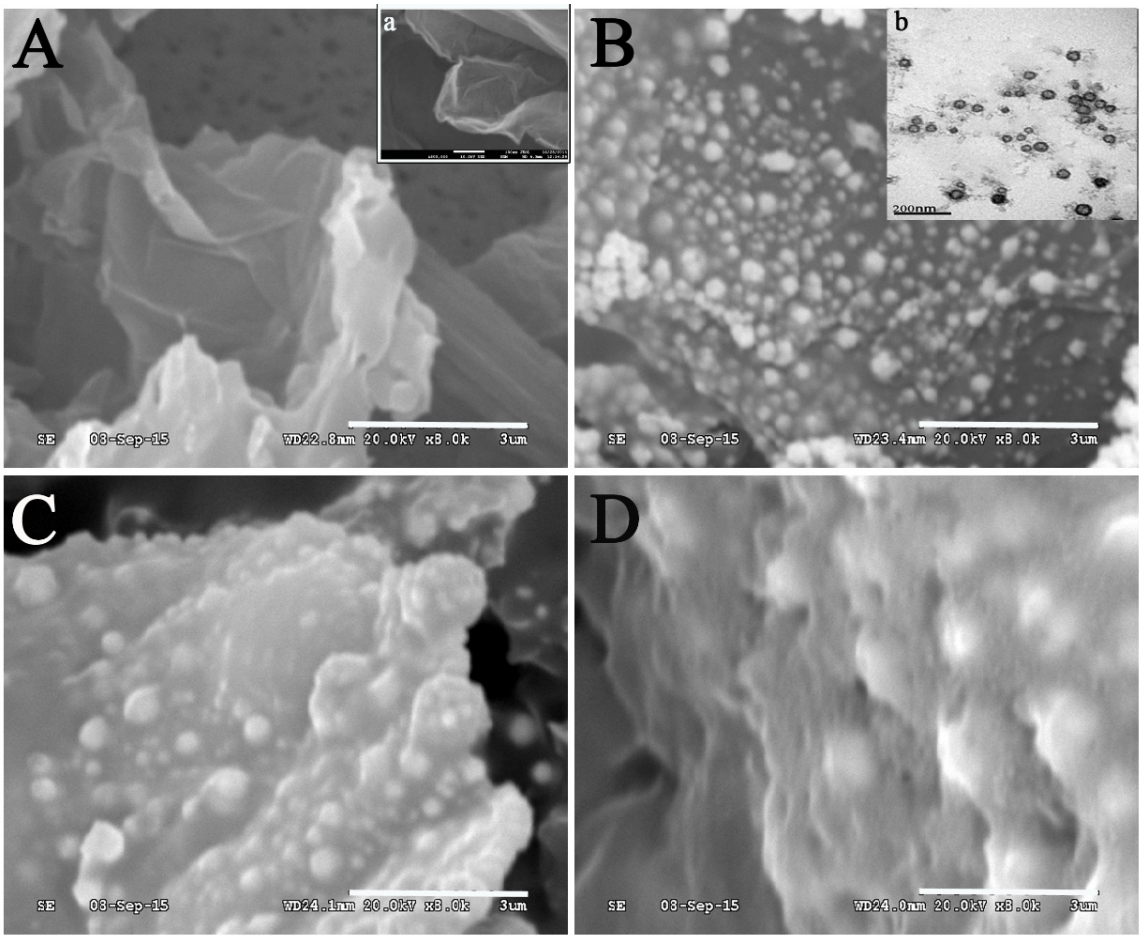

Figure 1(A-D): SEM images of **(A)** rGO-TEPA, **(B)** rGO-TEPA/Au PNPs, **(C)** rGO-TEPA/AuPNPs/streptavidin, and **(D)** rGO-TEPA/Au PNPs/streptavidin/PNA probe. The inset of (a) shows the FE-SEM image of rGO-TEPA; The inset of (b) shows the TEM image of Au PNPs.

Electrochemical Behavior of DNA Sensors

The electrochemical characteristics of different nanomaterials were investigated. It is clearly seen in (Figure 2A) that the electrode when modified by rGO-TEPA as compared with glassy-carbon electrode (curve a), and the electrode modified by Graphene Sheet (GS) (curve b), caused significantly increased currents (current c).

To investigate whether the Au PNPs were necessary for increasing the electron transferring of the DNA sensors, we challenged the GCE with Au PNPs, rGO-TEPA and rGO-TEPA/Au PNPs. As seen in (Figure 2B), the signal observed in single rGO-TEPA (curve b) and Au PNPs (curve c) were significantly lower than the composite of rGO-TEPA/Au PNPs (curve d). These results clearly show that for the sensitive detection of target DNA, the presence of Au PNPs is essential. Because the Au PNPs facilitate the electron transfer of the sensor, thus amplifying the electrochemical signal.

Owing to Au PNPs can facilitate the electron transfer of the sensor, thus Au PNPs were electrodeposited on the surface of rGO-TEPA to amplify the electrochemical signal. The deposition curve is shown in (Figure 2C). Increasing the deposition time resulted in a fast increase of the current responses, followed by a flat response at approximately 30 s. This indicated that the maximum deposition of Au PNPs was obtained. To evaluate whether Au PNPs have been successfully deposited on rGO-TEPA/GCE surface, we investigated the Cyclic Voltammetry (CV) of the rGO-TEPA modified electrode and rGO-TEPA/Au PNPs modified electrode in a 0.5 M H_2SO_4 solution. The peaks are associated with the reduction of oxide species on the electrode surface and can be used to determine the surface composition [23]. The peak at approximately 0.9 V corresponded to Au species [24]. As shown in (Figure 2D). no peak was obvious for the rGO-TEPA modified electrode (curve a), while the rGO-TEPA/Au PNPs (curve b) generated an obvious peak at 0.9 V in a 0.5 M H_2SO_4 solution, demonstrating that Au PNPs

had been successfully deposited on the rGO-TEPA/GCE surface. Meanwhile, using the Randles–Sevcik equation, the surface area of the rGO-TEPA/Au PNPs modified electrode is 4.81 times than that of the rGO-TEPA/GCE.

To monitor the modification procedure of the electrodes, CV experiments were performed in a 5 mM $[Fe(CN)_6]^{3-/4-}$ solution. As shown in (Figure 2E). A pair of typical reversible redox peaks of ferricyanide ions can be observed on the bare GCE (curve a). After the electrode was modified with rGO-TEPA, the peak current of the CV increased (curve b) due to the excellent electrical conductivity of rGO-TEPA. After Au PNPs were electrodeposited on the above electrode, the peak current further increased (curve c), implying that Au PNPs promote electron transfer. When the modified electrode was incubated with streptavidin (curve d), the peak current decreased due to the poor conductivity of streptavidin. When the modified electrode was immobilized with a biotinylated PNA probe (curve e), the peak current decreased due to the specific recognition between streptavidin and the biotinylated PNA probe, which hindered electron transfer. The peak current sharply declined after the sensor was blocked with MCH (curve f) due to the formation of a hydrophobic layer.

EIS is one of the most powerful tools for probing the features of surface– modified electrodes. Therefore, to further illustrate that all of the fabrication steps were effective, the electrochemical behaviours were characterized by electrochemical impedance spectroscopy using a 5 mM $[Fe(CN)_6]^{3-/4-}$ solution. It is well-known that the semicircle diameter in EIS is equal to the electron transfer resistance (R_{et}) and that the linear part of the curve at low frequency represents the diffusion process. As shown in (Figure 2F). when rGO-TEPA was modified onto the electrode, the resistance decreased (curve b) compared with the bare GCE (curve a), indicating that rGO-TEPA accelerated the electron transfer of the electrode. When Au PNPs were electrodeposited onto the electrode, the resistance decreased (curve c), indicating that Au PNPs promoted electron transfer between the electrode and the solution. Afterwards, a large semicircle diameter was observed when streptavidin was dropped onto the electrode (curve d), implying that streptavidin was successively immobilized onto the electrode. This larger diameter might be attributed to an insulating layer of proteins hindering the diffusion of electrons between the electrolyte and the electrode surface. After the electrode was incubated with the biotinylated PNA probe (curve e), the R_{et} increased dramatically due to the nonconductive property of DNA. Subsequently, with MCH blocked onto the electrode, the resistance increased (curve f), indicating that the sensors had indeed been successfully fabricated.

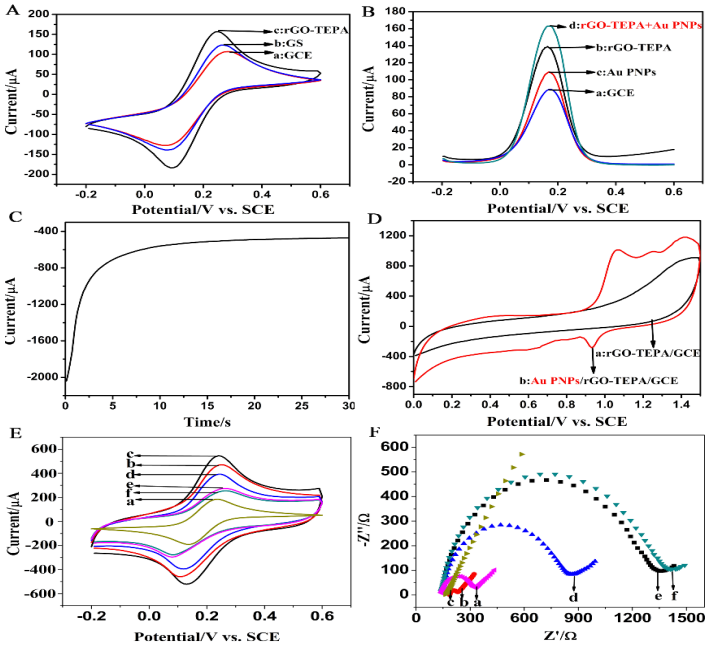

Figure 2(A-F): (A) The CVs of (a) bare GCE, (b) GS/GCE, and (c) rGO-TEPA/GCE in a 5 mM $[Fe(CN)_6]^{3-/4-}$ solution containing a 0.1 M KCl solution. **(B)** DPV responses of the DNA sensor of different modification steps: (a) bare GCE; (b) GCE/rGO-TEPA; (c) GCE/Au PNPs; and (d) GCE/ rGO-TEPA/Au PNPs in 5 mM $[Fe(CN)_6]^{3-/4-}$ containing a 0.1 M KCl solution. **(C)** The deposition curve of Au PNPs. **(D)** CV curves of GCE/ rGO-TEPA before (a) and after (b) deposition of porous gold nanoparticles in 0.5 M H_2SO_4 from 0 to 1.5 V at a scan rate of 100 mV/s. **(E)** CV characterization of electrodes at various stages of modification in a 5 mM $[Fe(CN)_6]^{3-/4-}$ solution containing 0.1 M KCl: (a) bare GCE, (b) GCE/ rGO-TEPA, (c) GCE/rGO-TEPA/Au PNPs (d) GCE/rGO-TEPA/Au PNPs/ streptavidin, (e) GCE/rGO-TEPA/Au PNPs/streptavidin/PNA probe, (f) GCE/rGO-TEP/AuNPs/AuPNPs/streptavidin/PNA probe/MCH; **(F)** EIS for each immobilization step in 5 mM $[Fe(CN)_6]^{3-/4-}$ containing a 0.1 M KCl solution: (a) bare GCE, (b) GCE/rGO-TEPA, (c) GCE/rGO-TEPA/Au PNPs (d) GCE/rGO-TEPA/Au PNPs/streptavidin, (e) GCE/ rGO-TEPA/Au PNPs/streptavidin/PNA probe, (f)GCE/rGO-TEPA/Au PNPs/streptavidin/PNA probe/MCH in 5 mM $[Fe(CN)_6]^{3-/4-}$ containing a 0.1 M KCl solution.

To validate that the signal amplification of our DNA assay, we investigated the dependence of the electrochemical signal on streptavidin. As expected, a significant signal change was observed in the presence of streptavidin (curve b) compared to the absence of streptavidin (curve a), shown in (Figure 3A). This results clearly show that for the sensitive detection of COX-1 DNA, the presence of streptavidin is essential. To verify the electrocatalytic current of the DNA sensors is dependent on the presence of target COX-1 DNA, we tested the modified sensors with and without target

DNA. As shown in (Figure 3B). the signal monitored at rGO-TEPA/Au PNPs/GCE modified with a probe sequence complementary to a portion of the target COX-1 gene significantly increases after exposure of the electrode to a synthetic target oligonucleotide (curve c). While, for the experiment in which target DNA was not introduced to the electrode (curve b), the voltammetric peak currents dropped to the background level (curve a), indicating that the current change is dependent on target COX-1 DNA.

In order to evaluate the catalytic efficiencies achieved with redox reporter system, we compared the catalytic current using the redox reporter, $Ru(NH_3)_6^{3+}$, with and without the catalytic enhancement provided by MPA and Cys (Figure 3C). shows the typical Differential Pulse Voltammetry (DPV) measurements. No considerable catalytic currents were observed for single $Ru(NH_3)_6^{3+}$ (curve a), however, the catalytic current for $Ru(NH_3)_6^{3+}$ is successively amplified in the presence of MPA (curve b, more than 4 times) and MPA combined Cys (curve c, more than 6 times), owing to MPA and Cys creates multiple redox cycles for a single $Ru(NH_3)_6^{3+}$ molecule and thus amplifies the observed current.

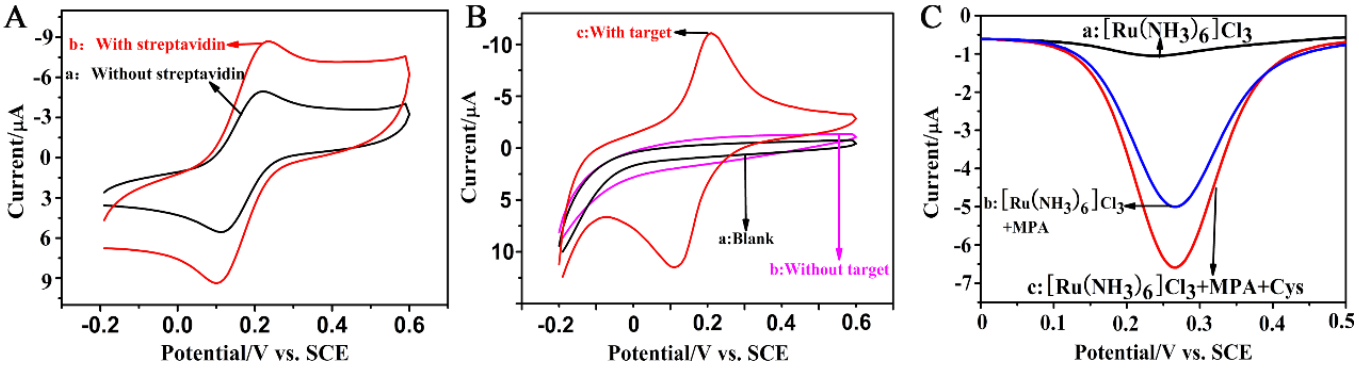

Figure 3(A-C): (A) Cyclic voltammograms of the electrodes without (curve a) and with (curve b) streptavidin modification in 5 mM $[Fe(CN)_6]^{3-/4-}$ containing a 0.1 M KCl solution. **(B)** Cyclic voltammograms of the modified electrode before (curve b) and after (curve c) hybridization with target DNA in 5 mM $[Fe(CN)_6]^{3-/4-}$ containing a 0.1 M KCl solution. **(C)** Different Pulse Voltammetry (DPV) scans of DNA sensors modified with PNA/DNA duplexes and incubated in 10 μM $Ru(NH_3)_6Cl_3$ for 60 s and then measured in a solution of 50 mM Tris buffer solution pH 9 (curve a), containing 0.5 mM 3-Mercaptopropionoic Acid (MPA) (curve b) as catalytic enhancer, and containing 0.5 mM 3-mercaptopropionoic acid (MPA) and 0.5 mM cysteamine (curve C) as catalytic enhancer.

Optimization of Experimental Conditions

To ensure the high performance of the DNA sensor, several parameters involved in the experiments, such as the concentration of rGO-TEPA, deposition time of Au PNPs, concentration of streptavidin, concentration of PNA probe, immobilization time of PNA probe and incubation time were investigated. As shown in (Figure 4A). the current response increased rapidly with increasing rGO-TEPA concentrations from 0.5 mg mL^{-1} to 2.0 mg mL^{-1}. A further increase in the concentration of rGO-TEPA decreased the current change, possibly because the excessive amount of rGO-TEPA decreased the surface area of the electrode and deterred electron transfer. Thus, 2.0 mg mL^{-1} of rGO-TEPA was used for electrode modification. In addition, the deposition time of the Au PNPs was investigated. As shown in (Figure 4B), the current response increased with the increasing the deposition time of Au PNPs from 5 s to 30 s, and then, the current response decreased with further deposition time increases. As a result, the electrode exhibited the highest current response at a deposition time of 30 s, possibly because the excessive amount of Au PNPs decreased the surface area of the electrode and deterred electron transfer. Therefore, the optimal deposition time of the Au PNPs was 30 s.

The concentration of streptavidin is another important factor influencing the DNA sensor response. Hence, the concentration of streptavidin is shown in (Figure 4C). With an increase in the concentration of streptavidin, the current responses first increased and then started to level off. The maximum current response appeared at 100 ng mL^{-1}. Therefore, 100 ng mL^{-1} was chosen as the optimal concentration of streptavidin. Furthermore, to achieve an optimal electrochemical signal, the concentration of PNA probe was systematically tested (Figure 4D). shows that the current response increased beginning at a concentration of 0.1 nM, reached a maximum value at a concentration of 10 nM, and then decreased up to a concentration of 20 nM. The results suggested that the best concentration was 10 nM. Therefore, this concentration (10 nM) was chosen for subsequent research.

To evaluate the immobilization time of PNA probe, we investigated the current responses by varying the immobilization time of 100 pg mL^{-1} target DNA. As shown in (Figure 4E). with the increase of immobilization time, the current responses for the DNA sensor first increased quickly and then remained steady at approximately 10 h, indicating that the maximum immobilization of DNA sensor was obtained. To completely hybridize the target DNA

in the following step, 10 h was chosen as the optimal immobilization time. Moreover, to obtain an optimal electrochemical signal, the incubation time was investigated, as shown in (Figure 4F). For the reason that it would take time to reach the maximum formation of the PNA/DNA complexes, the current responses increased with the increasing of incubation time. As the formation of PNA/DNA complexes getting saturated, the current responses start to level off after 60 min. Therefore, 60 min was chosen as the optimal incubation time.

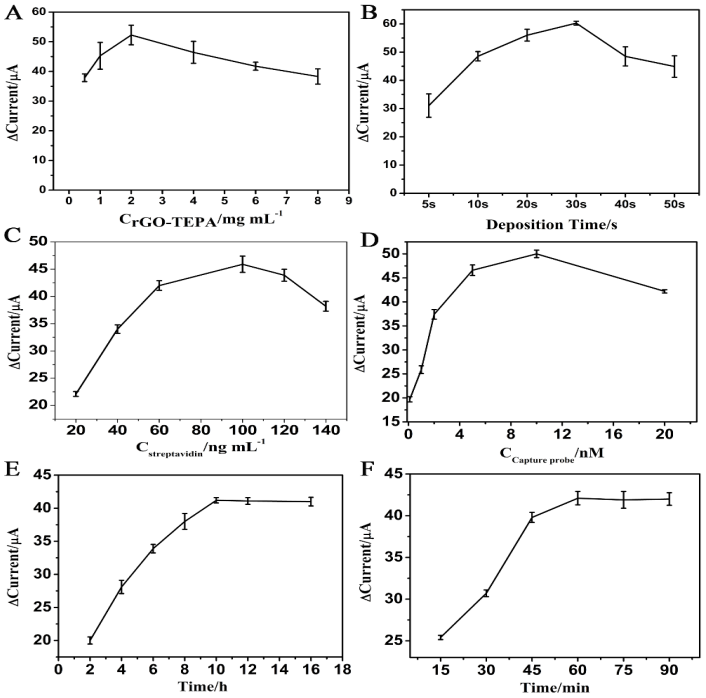

Figure 4(A-F): Effects of **(A)** the concentration of rGO-TEPA, where n = 10 for each point. **(B)** deposition time of Au PNPs, where n = 10 for each point. **(C)** concentration of streptavidin and **(D)** PNA probe, where n = 10 for each point. **(E)**immobilization time of PNA probe on the modified electrode, and **(F)** incubation time, where n = 10 for each point.

5Analytical performance of the DNA Sensor

To evaluate the sensitivity and quantitative range of the DNA sensor under the optimal assay conditions, the performance of the DNA sensor was evaluated with different concentrations of target DNA. As indicated in (Figure 5A), the DPV peak currents increased along with increasing concentrations of target DNA in the sample solution. The sample solution containing 3 mL of the 10-fold-diluted human serum sample was used for these experiments. For quantification, we measured the DPV peak currents variation ΔI ($\Delta I = I_{after} - I_{before}$, where I_{after} = current after target binding and I_{before} = current before target COX-1 binding). The calibration plots showed a good linear relationship between the peak currents (ΔI) and logarithmic values of the analyte concentrations over the range of 10 fM to 1 nM, as shown in (Figure 5B). The linear regression equation was ΔI (μA) =0.6827 Lg C + 0.8343 [COX-1] (M) (R^2 = 0.99). The detection limit of the method was estimated to be 2.8 fM at a signal-to-noise ratio of 3σ (where σ is the standard deviation of the blank, n = 8). The lower detection limit is attributed to the streptavidin-biotin system and the ECC redox cycling. Moreover, our strategy is technically simple and obviated the use of nanomaterials or multi-enzymes for signal amplification, reducing the operation complexity and assay cost.

Specificity, Reproducibility and Stability of the DNA Sensors

To investigate whether the DNA sensors could accurately interrogate a point-mutation, we challenged the DNA sensors with other oligonucleotides, such as single-base mismatch, three-base mismatch, non-complementary sequence and blank sample (a 10-fold-diluted healthy human serum sample). The responses of the DNA sensors were measured and are shown in (Figure 5C). Athough hybridization and washing were performed at elevated procedure, compared with the current response obtained from 1 nM COX-1, the responses caused by the mismatch sequences (1 nM for each one) were weak and negligible and were as low as the blank current. This indicated the high affinity of the DNA sensors to its complementary DNA target and that the developed DNA sensors could discriminate different DNA sequences effectively. A nearly negligible current change was obtained, which indicated that the developed biosensor could potentially be used in clinical application.

To assess the reproducibility of the DNA sensors, the fabricated electrodes were assessed by intra- and inter-assay Relative Standard Derivations (RSDs), as shown in (Figure 5D) and (Table S2). The intra-assay precision of the developed DNA sensors was calculated by detecting three samples containing 0.01, 1, and 100 pM of COX-1. Each sample was measured five times using five DNA sensors prepared in parallel. For different concentrations of COX-1, the intra-assay RSD values were less than 3.97 %. The inter-assay precision was estimated by measuring one sample with three DNA sensors that were independently formed at the same GCE, the RSD values were less than 4.22 % for different concentrations of COX-1. These results indicate that the proposed DNA sensors possesses acceptable precision and reproducibility.

COX-1		0.01	1	100
RSD (%)	Intra-assay	3.97	3.22	3.03
	Inter-assay	4.07	4.22	2..95

Table S2: Reproducibility of the electrochemical detection of COX-1.

To evaluate the stability of the DNA sensors, we investigated long-term storage. The DNA sensors were stored at 4°C when it was not in use and measured periodically. As shown in (Figure

5E), no obvious changes were observed during the first 3 days of storage, and the current changed by less than 1.6 %. In addition, we found that the electrode remains 97.2 % of its initial response to 10 pM targets for 7 days of storage and only loses 18.9 % of its sensing ability after one month of storage. Thus, the proposed DNA sensors has satisfactory stability.

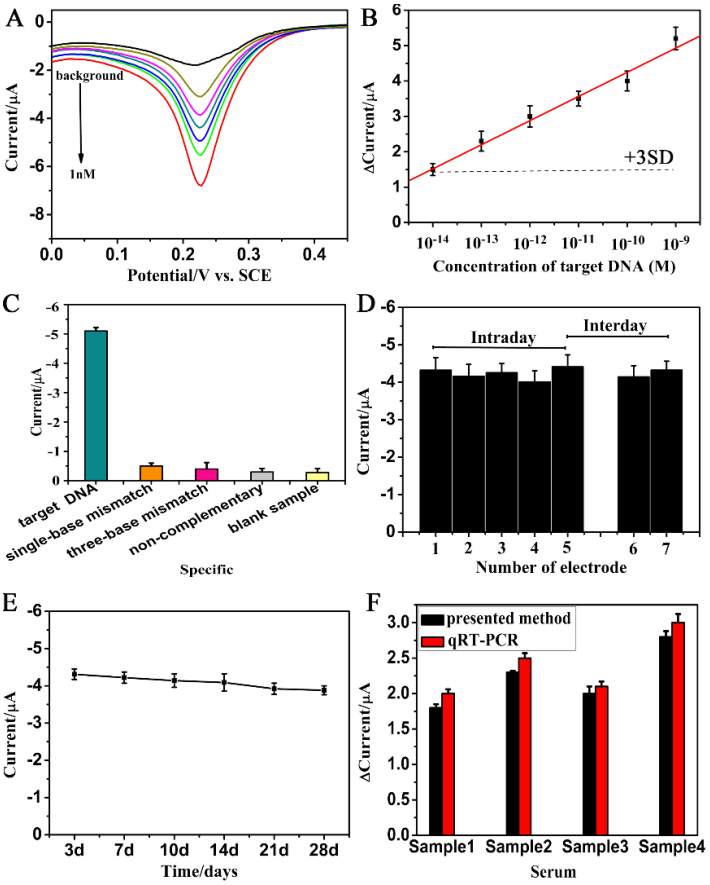

Figure 5(A-F): (A) DPV signals of the DNA sensors in the presence of different concentrations of COX-1 and **(B)** the calibration curve of the DNA sensors for 10 fM, 100 fM, 1 pM, 10 pM, 100 pM, 1 nM of COX-1 (n = 3). **(C)** Specific response of the DNA sensors hybridized with complementary COX-1, single-base mismatch, three-base mismatch, non-complementary and blank sample (100 pM for each analyse). **(D)** Reproducibility of 7 different electrodes modified with 100 pM of VKORC1. **(E)** The stability of the COX-1 DNA sensors (100 pM) after 3 d, 7d, 10 d, 14 d, 21 d, and 28 d. **(F)** Electrochemical currents of COX-1 in four serum samples detected by the presented method (black bars) and qRT-PCR (red bars), respectively.

Patient-Sample Analysis

To test the potential application of the DNA sensors for practical analysis, the DNA sensors were used to test the recovery of three concentrations of COX-1 in human serum samples, referencing the reported methods. Three concentrations (10 fM, 1 pM and 1 nM) of COX-1-spiked human serum samples were prepared by the standard addition method. The serum samples were diluted to suitable concentrations with pH 7.4 PBS (1:10). It can be observed from (Table S3) that the relative standard deviations were in the range of 2.249 to 3.778% and that the recoveries were in the range of 87.70 to 101.21%. These results show that the developed DNA sensors might be preliminarily applied to determine the presence of COX-1 in real samples.

Samples	Added	Found*	Recovery	RSD
			(%)	(%)
Sample-1	0.01 pM	0.877 pM	87.7	3.778
Sample-2	01:00 PM	0.998 pM	99.8	3.012
Sample-3	100 pM	101.21 pM	101.21	2.249
Samples (1-3) were from healthy people.				
*The values shown here are the average values from five measurements.				

The ultimate goal of developing a mutation-discriminating DNA sensor was to enable the direct analysis of mutated sequences in patient samples. We challenged our DNA sensors with the task of analysing COX-1 gene in serum samples from four patients who were treated invalidly with aspirin. Ten microliter samples of the four different patients were used. Each human serum sample was measured 5 times. As illustrated in (Figure 5F), the DNA sensors showed different current response for each of the patient serum sample. From the current response, the concentrations of COX-1 in the four different invalidly treated patients with aspirin were calculated to be 23.7 fM (Sample 1, Patient 1), 96.2 fM (Sample 2, Patient 1), 54.5 fM (Sample 3, Patient 3) and 272.8 fM (Sample 4, Patient 4), respectively. To ascertain the correctness of the results, we also tested the COX-1 contents with qRT-PCR. The results shown in Fig. 5F indicated that the levels of COX-1 in three real samples obtained by our method and qRT-PCR were of the same order of magnitude. Thus, the results indicated that the proposed DNA sensors could easily determine different concentrations of COX-1 and showed a high sensitivity.

Conclusion

In this paper, a novel and ultrasensitive electrochemical DNA sensor for the detection of COX-1 was prepared using ECC redox cycling. The proposed method has the following advantages: (1) a neutral charge biotinylated Peptide Nucleic Acid (PNA) probe modify the electrode surface can minimize the background current and increase the signal-to-noise ratio; (2) the newly introduced chemical regents of MPA and cysteamine not only permit Ru $(NH)^{3+}$ to be regenerated for multiple redox cycles but also overcome the interfering redox reactions near the potential of interest; (3) the detection limit is low. The low detection limit indicates that this approach is applicable to clinical pre-administration detection.

Accordingly, this methodology could simplify and speed up the identification of drug-susceptible people, saving medical resources and reducing time to treatment. Although we have focused on the detection of COX-1 mutations for aspirin, the DNA sensor can be extended to other relevant mutations recurring in other types of medicine-related gene. So, the presence of multiple mutations may be interrogated simultaneously, allowing a more detailed and precision clinical administration.

Acknowledgements

The research was financed by the Science and technology project of Sichuan provincial health and Family Planning Commission (No. 16PJ550).

References

1. Ornelas A, Millward NZ, Menter DG, Davis JS, Lichtenberger L, et al. (2017) Beyond COX-1: the effects of aspirin on platelet biology and potential mechanisms of chemoprevention. Cancer Metastasis Rev 36: 289-303.

2. Patrono C (2003) Aspirin resistance: definition, mechanisms and clinical read□outs. Journal of Thrombosis and Haemostasis 1: 1710-1713.

3. Xue M, Yang X, Yang L, Kou N, Miao Y, et al. (2017) Rs5911 and Rs3842788 Genetic Polymrphism, Blood Stasis Syndrome, and Plasma TXB2 and Hs-Crp Levels Are Associated With Aspirin Resistance in Chinese Chronic Stable Angina Patients. Evid Based Complement Alternat Med 2017:2322-2330.

4. Xue M, Yang L, Kou N, Miao Y, Wang M, et al. (2015) The Effect of Xuefuzhuyu Oral Liquid on Aspirin Resistance and Its Association with rs5911, rs5787, and rs3842788 Gene Polymorphisms. Evidence-Based Complementray and Alternative Me 2015: 507349.

5. Nojoomi F, Vafaei M, Bagheri Z, Zamanian Z (2017) Evaluation of Aspirin Effect on Candida Glabrata Isolates. MOJ Immunol 5: 00173.

6. Poon RWS, Tam EWT, Lau SKP, Cheng VCC, Yuen KY, et al. (2017) Molecular identification of cestodes and nematodes by cox1 gene real-time PCR and sequencing. Diagn Microbiol Infect Dis 89: 185-190.

7. Hong N, Cheng L, Wei B, Chen C, He LL, et al. (2017) An electrochemical DNA sensor without electrode pre-modification. Biosensors & Bioelectronics 91 :110-114.

8. Hu C, Kalsi S, Zeimpekis I, Sun K, Ashburn P, et al. (2017) Ultra-fast electronic detection of antimicrobial resistance genes using isothermal amplification and Thin Film Transistor sensors. Biosensors & Bioelectronics 96: 281-287.

9. Tee-Ngam P, Siangproh W, Tuantranont A, Vilaivan T, Chailapakul O, et al. (2017) Multiplex Paper-Based Colorimetric DNA Sensor Using Pyrrolidinyl Peptide Nucleic Acid-Induced AgNPs Aggregation for Detecting MERS-CoV, MTB, and HPV Oligonucleotides. sAnalytical Chemistry 89: 5428-5435.

10. Zhou YG, Wan Y, Sage AT, Poudineh M, Kelley SO (2014) Effect of Microelectrode Structure on Electrocatalysis at Nucleic Acid-Modified Sensors. Langmuir the Acs Journal of Surfaces & Colloids 30: 14322-14328.

11. Zhao Y, Hu S, Wang H, Yu K, Guan Y, Liu X, Li N, Liu F, Analytical Chemistry, 2017, Epub ahead of print.

12. D Voccia, M Sosnowska, F Bettazzi, G Roscigno, E Fratini (2017) Direct determination of small RNAs using a biotinylated polythiophene impedimetric genosensor. Biosensors & Bioelectronics 87: 1012-1019.

13. Yuan G, Yu C, Xia C, Gao L, Xu W, et al. (2015) A simultaneous electrochemical multianalyte immunoassay of high sensitivity C-reactive protein and soluble CD40 ligand based on reduced graphene oxide-tetraethylene pentamine that directly adsorb metal ions as labels. Biosensors & Bioelectronics 72: 237-246.

14. Chen L, Tremblay PL, Mohanty S, Xu K, Zhang T, (2016) Electrosynthesis of acetate from CO_2 by a highly structured biofilm assembled with reduced graphene oxide–tetraethylene pentamine. Journal of Materials Chemistry A 4: 8395-8401.

15. Li J, Yuan R, Chai YQ, Che X, Li W, et al. (2011) Nonenzymatic glucose sensor based on a glassy carbon electrode modified with chains of platinum hollow nanoparticles and porous gold nanoparticles in a chitosan membrane. Microchimica Acta s172: 163-169.

16. Liu L, Gao Y, Liu H, Du J, Xia N, (2014) Electrochemical-chemical-chemical redox cycling triggered by thiocholine and hydroquinone with ferrocenecarboxylic acid as the redox mediator. Electrochimica Acta 139: 323-330.

17. Xia N, Zhang Y, Wei X, Huang Y, Liu L (2015s) An electrochemical microRNAs biosensor with the signal amplification of alkaline phosphatase and electrochemical-chemical-chemical redox cycling. Analytica Chimica Acta 878: 95-101.

18. Han GC, Hou J, Feng XZ, Huang ZL, Gu W, et al. (2016) Electrochemical Determination of Protease with Improving Sensitivity by Electrochemical-chemical-chemical Redox Cycling. It. J. Electrochem. Sci 11: 8646–8653.

19. Das J, Ivanov I, Montermini L, Rak J, Sargent EH, et al. (2015) An electrochemical clamp assay for direct, rapid analysis of circulating nucleic acids in serum. Nature Chemistry 7: 569–575.

20. Besant JD, Das J, Burgess IB, Liu W, Sargent EH, et al. (2015) Ultrasensitive visual read-out of nucleic acids using electrocatalytic fluid displacement. Nature Communications 6: 6978-6985.

21. Wang Z, Liu N, Ma ZF (2014) Platinum porous nanoparticles hybrid with metal ions as probes for simultaneous detection of multiplex cancer biomarkers. Biosensors & Bioelectronics 53: 324-329

22. Zhang Q, Nordlander P, Wang H (2014) Porous Au Nanoparticles with Tunable Plasmon Resonances and Intense Field Enhancements for Single-Particle SERS. Journal of Physical Chemistry Letters 5: 370-374.

23. Ma H, Li X, Yan T, Li Y, Zhang Y, et al. (2015) Electrochemiluminescent immunosensing of prostate-specific antigen based on silver nanoparticles-doped Pb (II) metal-organic framework. Biosensors & Bioelectronics 79: 379-385.

24. Zhang H, Ma L, Li P, Zheng J (2016) A novel electrochemical immunosensor based on nonenzymatic Ag@Au-Fe_3O_4 nanoelectrocatalyst for protein biomarker detection. Biosensors & Bioelectronics 85: 343-350.